JAM CM Journal of Applied Mathematics and Computational Mechanics 2022, 21(2), 51-62
www.amcm.pcz.pl p-ISSN 2299-9965
DOI: 10.17512/jamcm.2022.2.05 e-ISSN 2353-0588

NUMERICAL ANALYSIS OF THERMAL DAMAGE AND OXYGEN DISTRIBUTION IN LASER IRRADIATED TISSUE

Marek Jasiński

Department of Computational Mechanics and Engineering
Silesian University of Technology
Gliwice, Poland
marek.jasinski@polsl.pl

Received: 24 November 2021; Accepted: 30 January 2022

Abstract. A numerical analysis of the thermal damage process that proceeds in biological tissue during laser irradiation is presented. Heat transfer in the tissue is assumed to be transient and two-dimensional. The internal heat source resulting from the laser irradiation based on the solution of optical diffusion equation is taken into account. Changes in tissue oxygen distribution resulting from temperature changes are analyzed using the Krogh cylinder model with Michaelis-Menten kinetics. A Hill model was used to describe the oxyhemoglobin dissociation curve. At the stage of numerical realization, the boundary element method and the finite difference method have been applied.

MSC 2010: *65M06, 65M38, 76Z05, 80A20, 80A99, 92C45*
Keywords: *bioheat transfer, optical diffusion equation, Arrhenius scheme, oxygen transport, Krogh cylinder, boundary element method, finite difference method*

1. Introduction

A variety of phenomena can occur in the tissue exposed to the laser irradiation, e.g. different chemical reactions and tissue damage resulting from temperature elevation. For the latter, the values of some thermophysical and optical parameters of the tissue can change [1, 2]. The perfusion coefficient and the scattering coefficient are particularly notable, which are often used as indicators of tissue damage. It is also worth noting that the perfusion coefficient, which changes its value under the influence of temperature or thermal injury, may indirectly affect other parameters related to blood flow, e.g., in capillaries, where oxygen passes to surrounding tissues. This means that the oxygen level in tissues changes together with increasing temperature and/or tissue damage [3].

The aim of this study was the numerical analysis of thermal damage of tissue under the impact of laser beam. In particular, the influence of thermal damage on the value of tissue parameters (perfusion and scattering coefficients) and on oxygen

transfer to the tissue was considered. In particular, two combined models are considered. The first one is related to the impact of the laser on biological tissue, resulting in an elevation in tissue temperature. As a result, the tissue undergoes thermal damage, whereby some tissue parameters are altered. The analysis was based on the Pennes bioheat transfer equation, laser energy deposition was estimated using the optical diffusion equation, while thermal damage was estimated based on the Arrhenius injury integral [2, 4, 5].

The variable perfusion coefficient was used to determine the capillary blood velocity, one of the basic parameters of the second model related to the oxygen distribution in the tissue. The geometry of this model is based on the concept of the Krogh cylinder, and the oxyhemoglobin dissociation curve in the form of the Hill model was taken into account. Two variants of calculations were taken into account: with and without the mitochondria clustering phenomenon. As is known, mitochondria are the main consumers of oxygen, which is necessary for the production of ATP. In case of oxygen deficiency, they tend to gather near capillaries, where access to oxygen is facilitated.

2. Governing equations

Transient heat transfer in the rectangular 2D homogeneous biological tissue domain Ω (Fig. 1 left) is described by Pennes bioheat transfer in the form [2, 6, 7]

$$\mathbf{x} \in \Omega: \quad c\dot{T} = \lambda \nabla^2 T + Q_{perf} + Q_{met} + Q_{las} \tag{1}$$

where T [K], λ [Wm^{-1}K^{-1}], c [Jm^{-3}K^{-1}] are the temperature, the thermal conductivity, volumetric specific heat of the tissue, respectively, while Q_{perf} [Wm^{-3}], Q_{met} [Wm^{-3}] and Q_{las} [Wm^{-3}] are the internal heat sources related to perfusion, metabolism and laser energy deposition. Equation (1) is supplemented by the convection boundary condition on the boundary Γ_0 (external surface of the tissue) and the adiabatic condition on the remaining part boundary Γ_c. The initial distribution of temperature is also known.

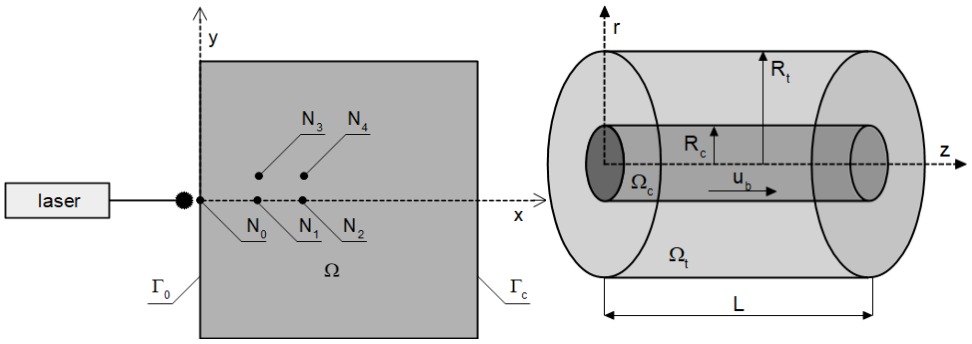

Fig. 1. The domains considered for the thermal and oxygen distribution model

The internal heat sources Q_{perf} and Q_{las} are described by the formulas [4-6]

$$Q_{perf}(\mathbf{x},t) = c_B w\left[T_B - T(\mathbf{x},t)\right], \quad Q_{las}(\mathbf{x},t) = \mu_a\left[\phi_c(\mathbf{x}) + \phi_d(\mathbf{x})\right]p(t) \tag{2}$$

where c_B [Jm^{-3}K^{-1}] is the volumetric specific heat of the blood, T_B corresponds to the arterial blood temperature, w [s^{-1}] is the perfusion coefficient, μ_a [m^{-1}] is the absorption coefficient, ϕ_c and ϕ_d [Wm^{-2}] are the collimated and diffuse parts of the total light fluence rate, respectively, while $p(t)$ is the function equal to 1 when the laser is *on* and equal to 0 when the laser is *off*.

The collimated fluence rate part ϕ_c is determined on the basis of the Beer--Lambert law, namely [1, 4]

$$\phi_c(\mathbf{x}) = \phi_0 \exp\left(-\frac{2x_2^2}{(d/2)^2}\right)\exp(-\mu_t' x_1) \tag{3}$$

where ϕ_0 [Wm^{-2}] is the surface irradiance of laser, d is the diameter of the laser beam, and μ_t' [m^{-1}] is the attenuation coefficient given as (μ_s' [m^{-1}] is the effective scattering coefficient)

$$\mu_t' = \mu_a + \mu_s' \tag{4}$$

To determine the diffuse fluence rate ϕ_d, the optical diffusion equation should be solved [8, 9]

$$\mathbf{x} \in \Omega: \quad \nabla \cdot \left[\frac{1}{3\mu_t'}\nabla\phi_d(\mathbf{x})\right] - \mu_a\phi_d(\mathbf{x}) + \mu_s'\phi_c(\mathbf{x}) = 0 \tag{5}$$

The elevation of tissue temperature due to laser energy deposition may result in thermal damage, the degree of which is determined by Arrhenius formula [4, 6, 10]

$$Arr(\mathbf{x},t^F) = \int_0^{t^F} A\exp\left[-\frac{E}{RT(\mathbf{x},t)}\right]\mathrm{d}t \tag{6}$$

where R [J mole^{-1}K^{-1}] is the universal gas constant, E [J mole^{-1}] is the activation energy and A [s^{-1}] is the preexponential factor. The criteria for tissue necrosis are $Arr(\mathbf{x}) \geq 1$ and/or $Arr(\mathbf{x}) \geq 4.6$.

Thermal tissue damage usually results in alteration of the values of some tissue parameters. In this work, the perfusion coefficient w and the effective scattering coefficient μ_s' are treated as thermally damage-dependent, and their values are estimated on the basis of the following formulas [5]

$$w(Arr) = w_0\sum_{i=0}^{2} m_i Arr^i, \quad \mu_s'(Arr) = \mu_{s\,nat}'\exp(-Arr) + \mu_{s\,den}'[1-\exp(-Arr)] \tag{7}$$

where w_0 [s^{-1}] is the initial perfusion coefficient, m_i are polynomial coefficients while $\mu'_{s\,nat}$ and $\mu'_{s\,den}$ are the values of the effective scattering coefficients for native and thermally damaged tissue.

In Figure 1 right, the oxygen distribution model is presented. This model is based on the concept of the Krogh cylinder in which R_c and R_t are the radiuses of the capillary and tissue cylinder, respectively, L is the length of the cylinder, u_b is the blood velocity in the capillary and r and z are the radial and axial coordinates.

The distribution of the partial pressure in the tissue subdomain P_t is described by the equation (in cylindrical coordinates) [11-15]

$$r \in \Omega_t: \quad K_t \nabla^2 P_t = M_t(P_t), \quad M_t(P_t) = \frac{M_0 P_t}{P_0 + P_t} \tag{8}$$

where K_t [($cm^2\ s^{-1}$)($cm^3_{O2}\ cm^{-3}\ mmHg^{-1}$)] is the Krogh diffusion coefficient, M_0 [$cm^3_{O2}\ cm^{-3}\ s^{-1}$] is oxygen demand while P_0 [mmHg] is the partial pressure that corresponds to half the maximum oxygen consumption. It should be pointed out that $M_t(P_t)$ is the oxygen consumption model in form of the Michaelis-Menten kinetics.

Equation (8) is supplemented by the following boundary conditions [11, 16]

$$\begin{aligned} r = R_c: &\quad 2\pi R_c K_t \nabla P_t(r) = -k\left[P_b - P_t(r)\right] \\ r = R_t: &\quad \nabla P_t(r) = 0 \end{aligned} \tag{9}$$

In the axial direction, the equation with initial condition is assumed [11]

$$Q_b \kappa_b \nabla S_{Hb}(P_b, z) = -k\left(P_b - P_t\right), \quad z = 0: \quad P_b = P_{b\,inlet} \tag{10}$$

where S_H is hemoglobin saturation, P_b [mmHg] is the partial pressure of oxygen in the capillary, Q_b [$cm^3\ s^{-1}$] denotes the blood flow rate in the capillary, while κ_b [$cm^3_{O2}\ cm^{-3}_{blood}$] is the oxygen carrying capacity of the blood at 100% saturation.

After the determination of the hemoglobin saturation S_{Hb} on the basis of (10), the partial pressure in the capillary P_b is estimated as the inversion of the Hill model of the oxyhemoglobin dissociation curve [14, 17, 18]

$$S_{Hb}(P_b) = \frac{P_b^n}{P_b^n + P_{50}^n} \quad \rightarrow \quad P_b = P_{50}\left(\frac{S_{Hb}}{1 - S_{Hb}}\right)^{\frac{1}{n}} \tag{11}$$

where n denotes the Hill coefficient while P_{50} is the pressure corresponding to 50% hemoglobin saturation.

As was already mentioned, the perfusion coefficient is assumed to be damage-dependent (cf. equation (7)), but changes in tissue perfusion also affect parameters associated with the oxygen distribution model. In the current work, it is assumed that (u_b denotes the blood velocity in capillary [cm s^{-1}]) [3, 11]

$$w = \frac{Q_b}{\pi R_t^2 L_t} = \frac{\pi R_c^2 u_b}{\pi R_t^2 L_t} \quad \rightarrow \quad u_b = w(Arr) L_t \frac{R_t^2}{R_c^2} \tag{12}$$

3. Method of solution

At the stage of numerical realization, the 1st scheme of the boundary element method (BEM) for the 2D transient bioheat equation has been used, while the optical diffusion equation and the oxygen distribution model have been solved by the finite difference method (FDM).

For the transient bioheat diffusion problem, the boundary integral equation corresponding to transition $t^{f-1} \rightarrow t^f$ is of the form (assuming constant time step Δt)

$$B(\xi)T(\mathbf{x},t^f) + \frac{1}{c}\int_{t^{f-1}}^{t^f}\int_{\Gamma} T^*(\xi,\mathbf{x},t^f,t)\, q(\mathbf{x},t)\,\mathrm{d}\Gamma\,\mathrm{d}t =$$

$$= \frac{1}{c}\int_{t^{f-1}}^{t^f}\int_{\Gamma} q^*(\xi,\mathbf{x},t^f,t)\, T(\mathbf{x},t)\,\mathrm{d}\Gamma\,\mathrm{d}t + \iint_{\Omega} T^*(\xi,\mathbf{x},t^f,t^{f-1})\, T(\mathbf{x},t^{f-1})\,\mathrm{d}\Omega + \tag{13}$$

$$+ \frac{1}{c}\int_{t^{f-1}}^{t^f}\iint_{\Omega} Q_V(\mathbf{x},t) T^*(\xi,\mathbf{x},t^f,t)\,\mathrm{d}\Omega\,\mathrm{d}t$$

where Q_V denotes the sum of internal heat sources associated with perfusion, metabolism, and laser irradiation (c.f. equation (1)), T^* and q^* are the fundamental solution and the heat flux resulting from the fundamental solution, respectively and $B(\xi)$ is the coefficient from the interval (0, 1). Detailed information on BEM can be found in [19].

To determine the source function Q_{las} at the internal nodes, for each time step, the optical diffusion equation (5) must be solved. For this reason, the FDM is applied. The global and local numeration of the nodes, which is assumed, is shown in Figure 2b.

The difference equation for the central node of the stencil can be written in the form

$$\phi_{d0} = \left(\sum_{e=1}^{4} \frac{\phi_{de}}{R_{0e}} + h\mu_s'\phi_{c0}\right) \Big/ \left(\sum_{e=1}^{4} \frac{1}{R_{0e}} + h\mu_a\right) \tag{14}$$

where R_{0e} are the resistances between the central node and the remaining nodes of the stencil.

In the oxygen distribution model, for the radial problem (cf. equations (8) and (9)) the finite difference method has also been applied with a grid based on three-point stencils (Fig. 2c). As the problem is non-linear, the Jacobian has been determined [3]

$$
\begin{aligned}
J_{i,i} &= -\left(\beta_{i-1}\frac{P_0 P_{t,i-1}}{P_{t,i}^2} + \beta_i + \beta_{i+1}\frac{P_0 P_{t,i+1}}{P_{t,i}^2}\right), \\
J_{i,i-1} &= \beta_{i-1}\frac{P_0 + P_{t,i}}{P_{t,i}}, \qquad J_{i,i+1} = \beta_{i+1}\frac{P_0 + P_{t,i}}{P_{t,i}}, \\
J_{0,0} &= -\left(\frac{2\pi R_c K_t}{h_r} + k\right), \qquad J_{0,1} = \frac{2\pi R_c K_t}{h_r}, \\
J_{nr,nr-1} &= \frac{1}{h_r}, \qquad J_{nr,nr} = -\frac{1}{h_r}
\end{aligned}
\tag{15}
$$

where nr is the number of nods in the radial direction, while

$$
\beta_{i-1} = \frac{1}{h_r^2}\frac{r_i - 0.5h_r}{r_i} \quad \beta_{i+1} = \frac{1}{h_r^2}\frac{r_i + 0.5h_r}{r_i} \quad \beta_i = \beta_{i-1} + \beta_{i+1} \tag{16}
$$

After the determination of the partial pressure in the tissue P_t in the radial direction for a given node m, the saturation S_{Hb} is calculated in the next node $m+1$ on the basis (cf. equation (10))

$$
S_{Hb,m+1} = -\frac{kh_z}{Q_b \kappa_b}\left(P_{b,m} - P_{t,m}\right) + S_{Hb,m}, \quad m = 0,1,...,nz \tag{17}
$$

where nz is the number of nodes in the axial direction. Then the partial pressure in the capillary P_b in node $m+1$ is also determined using equation (11).

More details on the numerical realization of the FDM can be found in [20, 21].

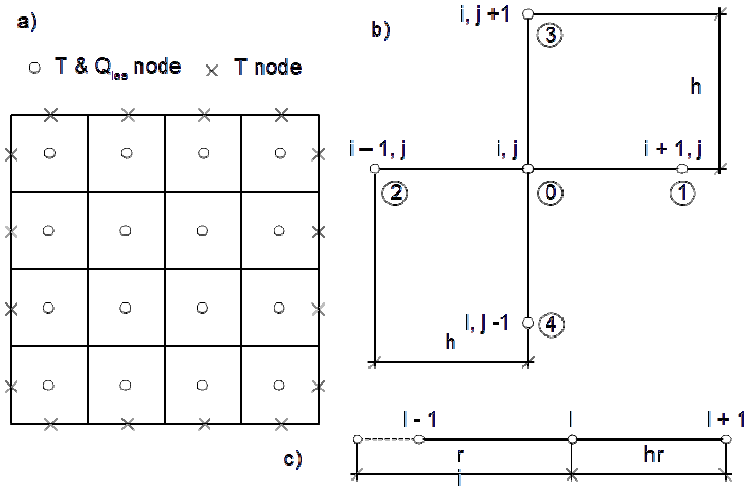

Fig. 2. Discretization for BEM (a) and stencils for optical task (b) and oxygen distribution task (c)

4. Results of calculations

In the first stage, the aim of the research was to analyze the destructive changes in tissue domain of the size 4×4 cm during laser irradiation (cf. Fig. 1 left). The interior of domain has been divided into 1600 internal constant cells, while the external boundary has been divided into 160 constant elements. In the calculations, the following values of the thermophysical and optical parameters of tissue and blood were assumed: $\lambda = 0.609$ Wm^{-1}K^{-1}, $c = 4.18$ MJm^{-3}K^{-1}, $w_0 = 0.005$ s^{-1}, $Q_{met} = 250$ Wm^{-3}, $\mu_a = 0.4$ cm^{-1}, $\mu'_{snat} = 10$ cm^{-1}, $\mu'_{sden} = 40$ cm^{-1}, $c_B = 3.9962$ MJm^{-3}K^{-1}, $T_B = 37$°C. It should be pointed out that the optical parameters of tissue (μ_a, μ'_{snat} and μ'_{sden}) are typical for near-IR irradiation on soft tissue, e.g. Nd:YAG laser of 1064 nm, which is used for prostate coagulation [5].

In the boundary-initial conditions for the thermal problem the following date were used: $\alpha = 10$ Wm^{-2}K^{-1} (convection coefficient), $T_{amb} = 20$°C (ambient temperature), $T_{init} = 37$°C (initial tissue temperature) while for the laser impulse: $\phi_0 = 30$ W cm^{-2}, $d = 2$ mm, $t_{exp} = 25$ s (duration of the laser impulse).

In the part of the model related to tissue damage, the data assumed were as follows: $A = 3.1$e+98 s^{-1}, $E = 6.27$e+5 J mol^{-1}, $R = 8.314$ J mol^{-1} K^{-1}, additionally, the polynomial coefficients in (7) were assumed as: $m_0 = 1$, $m_1 = 25$, $m_2 = -260$ for $0 \le Arr \le 0.1$, $m_0 = 1$, $m_1 = -1$, $m_2 = 0$ for $0.1 < Arr \le 1$ and $m_0 = m_1 = m_2 = 0$ for $Arr > 1$ [5].

For the oxygen distribution model, the data assumed were: $R_c = 3.25$ μm, $R_t = 32.5$ μm, $L = 162.5$ μm, $K_t = 9.4$e–10 (cm^2 s^{-1})(cm$^3_{O2}$cm^{-3} mmHg^{-1}), $M_0 =$ $= 1.12$e–3 cm$^3_{O2}$ cm^{-3} s^{-1}, $k = 6.25$e–9 (cm^2 s^{-1})(cm$^3_{O2}$ cm^{-3} mmHg^{-1}), $P_0 = 1$ mmHg, $P_{b\,inlet} = 100$ mmHg, $\kappa_b = 0.2$ cm$^3_{O2}$ cm$^{-3}_{blood}$, $n = 2.7$, $P_{50} = 26$ mmHg [11, 16, 17].

In the first step, the task related to determining the temperature distribution, tissue damage, and damage-dependent parameters was solved. Figures 3-5 are associated with tissue temperature and damage. In Figure 3 the distribution of temperature for 15, 25, and 60 s is presented, while in Figure 4 the Arrhenius integral distribution is shown. In Figure 5 the history of temperature and tissue damage at control points N_0-N_4 is shown (cf. Fig. 1 left). It is visible that the area of tissue damage continues to grow even after the laser pulse has stopped. This is due to the heat wave migrating into the tissue. The degree of tissue damage is calculated using the Arrhenius scheme, which assumes that the tissue damage is irreversible.

The value of the Arrhenius integral has an impact on the values of the perfusion coefficient and the effective scattering coefficient, which are presented in Figure 6 (cf. equation (7)). The perfusion coefficient increases at the early stage of the process when the temperature is moderate. It is due to vasodilation. Then, as tissue damage progresses, perfusion decreases due to vascular damage. For the effective scattering coefficient, the increase is visible along with the increase in tissue damage, which is usually associated with a visual effect of tissue ‘whitening’.

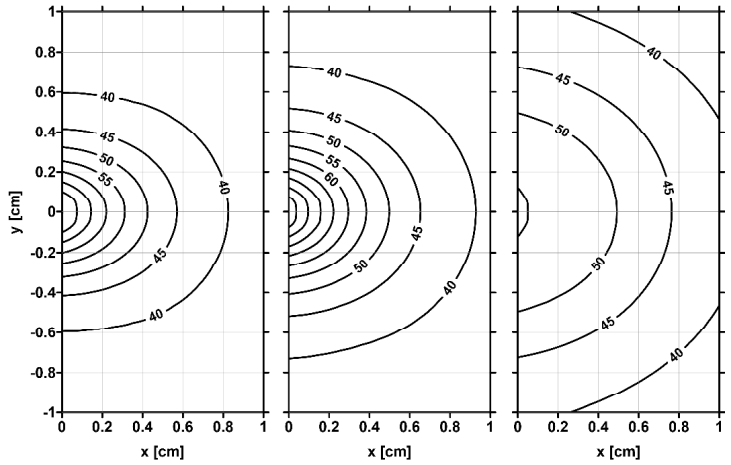

Fig. 3. Temperature distribution for time 15, 25 and 60 s

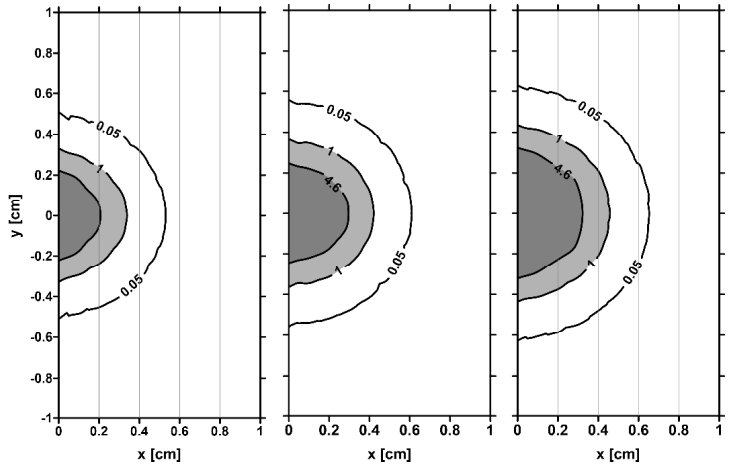

Fig. 4. Distribution of tissue damage for time 15, 25, and 60 s

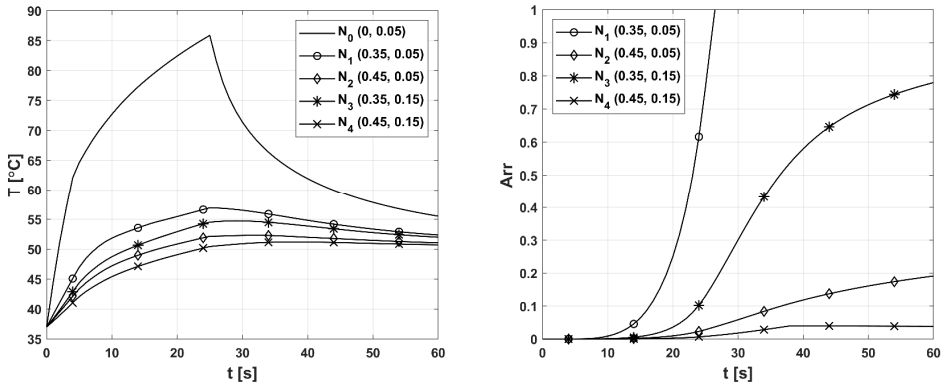

Fig. 5. History of temperature and Arrhenius integral at nodes N_0-N_4

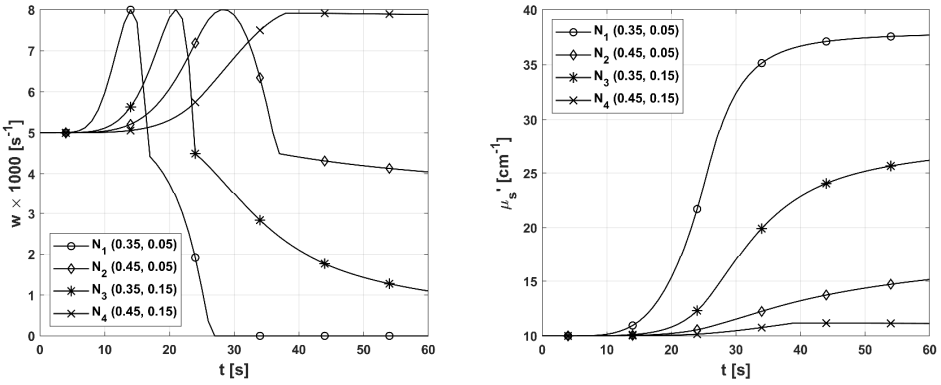

Fig. 6. History of perfusion coefficient w and effective scattering coefficient μ_s' at nodes N_0-N_4

Based on the history of the perfusion coefficient, the control point N_3 was chosen as the one in which the value of blood velocity in the capillary u_b is calculated (cf. Fig. 1 left, Fig. 6, equation (12)). At point N_3, the maximum perfusion value is reached at 21 s, then decreases to 0.0011 s^{-1} after 60 s, so it can be said that this point corresponds to an area of tissue not completely damaged.

Since the oxygen distribution model was assumed to be a steady-state problem, calculations were performed for selected times of the perfusion coefficient history, i.e. 0, 21, 20, 40, 50, 60 s. The results obtained are shown in Figure 7. For the radial direction, one curve is visible for $z = 0$, which was identical in each simulation (identical $P_{b\ inlet}$ value assumed in each simulation), while the remaining curves are for $z = L/2$. For the axial direction, the curves show the capillary pressure, i.e. P_b. They indicate the occurrence of hypoxia between 40 and 50 s.

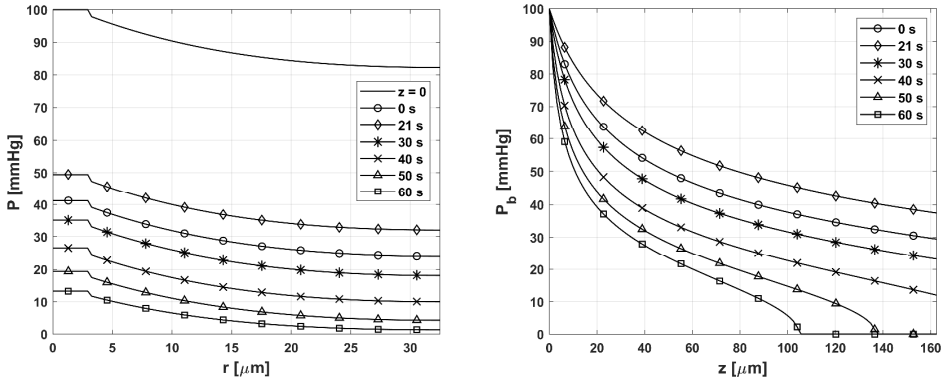

Fig. 7. Partial pressure of the oxygen distribution in the radial and axial directions

As already mentioned, calculations were also performed taking into account the phenomenon of mitochondria clustering [11]. The model incorporates this phenomenon by assuming two zones in the tissue subdomain. In the zone adjacent

to the capillary (i.e. for $R_c \le r \le (R_t - R_c)/2$) the value of oxygen demand $4 \times M_0$ were assumed while in the second zone (ie. for $(R_t - R_c)/2 < r \le R_t$): $M_0 = 0$.

Comparisons of the values obtained from the basic variant of the calculations, with the values of the calculations for the variant with clustering of mitochondria, are shown in Figure 8.

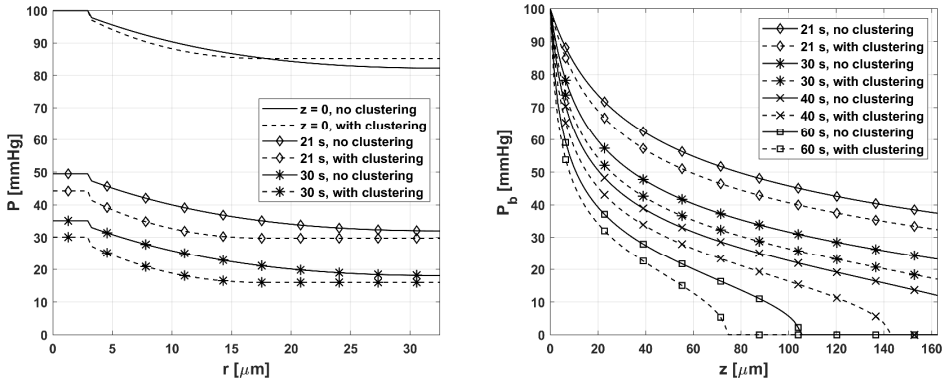

Fig. 8. Partial pressure of the oxygen distribution in radial and axial directions for the case with and without mitochondria clustering

5. Conclusions

The problem considered in this paper is a multiscale problem because the two models used different dimensions (millimeters for the thermal model vs. micrometers for the oxygen distribution problem). Therefore, one may say that the results show the effect of laser beam irradiation on biological tissue at different levels. For the thermal model, the tissue damage process and the resulting changes in the values of the perfusion coefficient and the effective scattering coefficient are shown. The values of capillary blood velocity u_b, one of the parameters of the oxygen distribution model, were determined on the basis of the first of these parameters.

The results show how changes in u_b affect the distribution of the partial pressure of oxygen both in the capillary and in the tissue surrounding the capillary. It should be noted that the partial pressure at the capillary entrance $P_{b\,inlet}$ was assumed to be a constant value. Under conditions of thermal injury and reduced perfusion, there is also damage to the vasculature that is closely related to decreased blood pressure. It is also worth noting that for the assumed damage-dependent perfusion coefficient function (cf. equation (7)), the range $0.1 < Arr \le 1$ corresponds to vasodilation which in the model related to the temperature distribution and determining the degree of tissue damage means an increase in perfusion, while in the oxygen distribution model it could mean a change in diameter of the capillary R_c.

Figure 8 shows a comparison of two computational variants – with and without mitochondria clustering. It can be seen that for the case including this phenomenon,

there is a greater decrease in the partial pressure of oxygen in the part of the tissue adjacent to the capillary. A larger decline in the axial direction is also seen, resulting in an earlier drop in P_b to zero, i.e. the occurrence of hypoxia.

Temperature also affects oxygen transport to the tissue through the so-called Bohr effect, i.e. an increase in temperature causes the right shift of the oxhemoglobin dissociation curve. Numerical analyses of this phenomenon have been presented in [3], while in the current work the ODC parameters i.e. P_{50} and n have been taken to be constant.

Finally, note that the current work considers the process of tissue damage due to elevated temperature. However, mixed photothermal and photochemical phenomena often occur with laser irradiation on tissue. This occurs, for example, during photodynamic therapy. For this reason, to reproduce these type of processes more accurately, the oxygen distribution model should be supplemented with equations related to chemical reactions in tissue [18]. Furthermore, due to the variation in individual characteristics, it seems reasonable to use sensitivity analysis methods or interval arithmetic.

Acknowledgements

The research is funded from the projects Silesian University of Technology, Faculty of Mechanical Engineering.

References

[1] Niemz, M.H. (2007). *Laser-tissue Interaction*. Berlin, Heidelberg, New York: Springer-Verlag.

[2] Paruch, M. (2018). Identification of the degree of tumor destruction on the basis of the Arrhenius integral using the evolutionary algorithm. *International Journal of Thermal Sciences*, *130*, 507-517.

[3] Jasiński, M. (2020). Numerical analysis of the temperature impact to the oxygen distribution in the biological tissue. *Journal of Applied Mathematics and Computational Mechanics*, *19*, 17-28.

[4] Korczak, A., & Jasiński, M. (2019). Modelling of biological tissue damage process with application of interval arithmetic. *Journal of Theoretical and Applied Mechanics*, *57*, 249-261.

[5] Jasiński, M. (2018). Modelling of thermal damage process in soft tissue subjected to laser irradiation. *Journal of Applied Mathematics and Computational Mechanics*, *17*, 29-41.

[6] Paruch, M. (2020). Mathematical modeling of breast tumor destruction using fast heating during radiofrequency ablation. *Materials*, *13*, 136.

[7] Mochnacki, B., & Ciesielski, M. (2016). Sensitivity of transient temperature field in domain of forearm insulated by protective clothing with respect to perturbations of external boundary heat flux. *Bulletin of the Polish Academy of Sciences – Technical Sciences*, *64*, 591-598.

[8] Dombrovsky, L.A. (2012). The use of transport approximation and diffusion-based models in radiative transfer calculations. *Computational Thermal Sciences*, *4*(4), 297-315.

[9] Dombrovsky, L.A., Randrianalisoa, J.H., Lipinski, W., & Timchenko, V. (2013). Simplified approaches to radiative transfer simulations in laser induced hyperthermia of superficial tumors. *Computational Thermal Sciences*, *5*(6), 521-530.

[10] Narasimhan, A., & Sadasivam, S. (2013). Non-Fourier bio heat transfer modelling of thermal damage during retinal laser irradiation. *International Journal of Heat and Mass Transfer*, *60*, 591-597.

[11] McGuire, B.J., & Secomb, T.W. (2001). A theoretical model for oxygen transport in skeletal muscle under conditions of high oxygen demand. *Journal of Applied Physiology*, *91*, 2255--2265.

[12] Fry, B.C., Roy, T.K., & Secomb, T.W. (2013). Capillary recruitment in a theoretical model for blood flow regulation in heterogeneous microvessel networks. *Physiological Reports, 1*(3), e00050.

[13] Goldman, D. (2008). Theoretical models of microvascular oxygen transport to tissue. *Microcirculation*, *15*, 795-811.

[14] Popel, A.S. (1989). Theory of oxygen transport to tissue. *Critical Reviews in Biomedical Engineering*, *17*, 257-321.

[15] He, Y., Shirazaki, M., Liu, H., Himeno, R., & Sun, Z. (2006). A numerical coupling model to analyze the blood flow, temperature, and oxygen transport in human breast tumor under laser irradiation. *Computers in Biology and Medicine*, *36*, 1289-1378.

[16] McGuire, B.J., & Secomb, T.W. (2003). Estimation of capillary density in human skeletal muscle based on maximal oxygen consumption rates. *American Journal of Physiology-Heart and Circulatory Physiology*, *285*, H2382-H2391.

[17] Whiteley, J.P., Gavaghan, D.J., & Hahn, C.E.W. (2002). Mathematical modelling of oxygen transport to tissue. *Journal of Mathematical Biology*, *44*, 503-522.

[18] Zhu, T.C., Liu, B., & Penjweini, R. (2015). Study of tissue oxygen supply rate in a macroscopic photodynamic therapy singlet oxygen model. *Journal of Biomedical Optics*, *20*, 038001.

[19] Brebia, C.A., & Dominquez, J. (1992). *Boundary Elements, An Introductory Course* (*Computational Mechanics Publications*). London: McGraw-Hill Book Company.

[20] Mochnacki, B., & Piasecka-Belkhayat, A. (2013). Numerical modeling of skin tissue heating using the interval finite difference method. *Molecular & Cellular Biomechanics*, *10*, 233-244.

[21] Majchrzak, E., & Mochnacki, B. (2016). Dual-phase lag equation. Stability conditions of a numerical algorithm based on the explicit scheme of the finite difference method. *Journal of Applied Mathematics and Computational Mechanics*, *15*, 89-96.